Grain growth and phase stability of nanocrystalline cubic zirconia under ion irradiation

Yanwen Zhang,[1,*] Weilin Jiang,[1] Chongmin Wang,[1] Fereydoon Namavar,[2] Philip D. Edmondson,[1] Zihua Zhu,[1] Fei Gao,[1] Jie Lian,[3] and William J. Weber[4,5]

[1]*Pacific Northwest National Laboratory, P.O. Box 999, Richland, Washington 99352, USA*

[2]*University of Nebraska Medical Center, Omaha, Nebraska 68198, USA*

[3]*Rensselaer Polytechnic Institute, Troy, New York 12180, USA*

[4]*Department of Materials Science & Engineering, University of Tennessee, Knoxville, Tennessee 37996, USA*

[5]*Materials Science & Technology Division, Oak Ridge National Laboratory, Oak Ridge, Tennessee 37831, USA*

(Received 18 April 2010; revised manuscript received 5 October 2010; published 10 November 2010)

Grain growth, oxygen stoichiometry, and phase stability of nanostructurally stabilized cubic zirconia (NSZ) are investigated under 2 MeV Au-ion bombardment at 160 and 400 K to doses up to 35 displacements per atom (dpa). The NSZ films are produced by ion-beam-assisted deposition technique at room temperature with an average grain size of 7.7 nm. The grain size increases with irradiation dose to ~30 nm at ~35 dpa. Slower grain growth is observed under 400 K irradiations, as compared to 160 K irradiations, indicating that the grain growth is not thermally activated and irradiation-induced grain growth is the dominating mechanism. While the cubic structure is retained and no new phases are identified after the high-dose irradiations, oxygen reduction in the irradiated NSZ films is detected. The ratio of O to Zr decreases from ~2.0 for the as-deposited films to ~1.65 after irradiation to ~35 dpa. The loss of oxygen suggests a significant increase in oxygen vacancies in nanocrystalline zirconia under ion irradiation. The oxygen deficiency may be essential in stabilizing the cubic phase to larger grain sizes.

DOI: 10.1103/PhysRevB.82.184105 PACS number(s): 61.80.−x, 61.46.−w, 68.35.Rh

I. INTRODUCTION

Nanostructured materials with grain sizes well below 100 nm are leading to revolutionary advances in technology.[1–6] Due to their exotic structure and exceptional size-dependent control of chemical, physical, electrical and optical properties, nanostructured materials have attracted wide interest[1–5] in applications such as novel catalysis, sensors, membranes, bioimaging, solar cells, and advanced nuclear energy systems. As the world increases its reliance on nuclear energy, there is an ever-increasing demand for new radiation tolerant materials that can withstand the extreme radiation environments in reactors, accelerators, and even geologic repositories for nuclear waste. Understanding response of nanostructured materials to energy deposition is an urgent challenge, since it may hold the key to unlock the design of new materials for advanced nuclear energy systems.

Ceramics are critical engineering materials for electronic, space, and nuclear applications; and zirconium dioxide (ZrO_2) has been well studied due to its superior chemical, mechanical, and optical properties. Pure ZrO_2 has a monoclinic crystal structure at room temperature and reversibly transforms to tetragonal and cubic phases at increasing temperatures.[3,4,7] The monoclinic phase has little practical applications due to 3–5 % volume expansion during cooling. The tetragonal and cubic zirconia have attracted most attention as various coating materials, refractory materials, and dispersed phases in composite materials.[8] Cubic zirconia is isostructural with urania, plutonia, and thoria nuclear fuel compounds.[7] As a potential inert fuel matrix, zirconia must survive the harsh radiation environment within a nuclear reactor core. Thus, in the context of nuclear fuels and the transmutation of radioactive actinides, cubic zirconia is a model system for evaluating the role of nanograined structures on radiation effects. Knowledge on the response of nanograined cubic zirconia to ion irradiation will improve the understanding of defect production, interactions, and phase transition pathways in nanomaterials used in a radiation environment. More importantly, the ability to control and engineering materials by ion beams in a far from equilibrium environment, including nanostructure evolution and phase stability, may have profound impacts in research on new clean energy sources, sensors, and high-energy density batteries.

Ion-irradiation studies on zirconia have been mainly performed on partially or fully stabilized single crystals or materials with micron-size grains.[7,9–11] Studies of irradiation effects in nanocrystalline zirconia have been carried out using either nanopowders with free surfaces or nanoparticles embedded in a surrounding foreign matrix with inhomogeneous interfaces.[8] Recently, the irradiation-induced amorphous to tetragonal phase transformation in nanocrystalline zirconia has been reported.[3] The current work focuses on the irradiation response of nanostructurally stabilized cubic zirconia (NSZ) in the form of a homogeneous nanograined film, and the results should provide insights on nanostructure evolution and phase stability under far from equilibrium conditions.

II. EXPERIMENTAL PROCEDURE

Stabilizer-free cubic zirconia films with grain sizes ranging from 5 to 10 nm were grown on a Si(100) wafer using an ion-beam-assisted deposition (IBAD) system (Mill Lane Engineering, Lowell, MA).[4] These NSZ films have been shown to be thermally stable up to 1123 K.[4,6] The nanostructural evolution and phase stability of the NSZ films under irradiation are investigated using 2 MeV Au ions, which maximize the deposited energy and minimize the implanted ion content

for a given displacement damage level compared to light ion irradiations. Energy of 2 MeV is chosen so that most of Au ions penetrate the zirconia films and stop in the Si substrate. The zirconia films were irradiated at 160 and 400 K to ion fluences up to 1×10^{16} cm^{-2}, with the ion flux maintained at $\sim4\times10^{11}$ cm^{-2} s^{-1}. The elemental composition and nanoscale structure of both the as-deposited and irradiated zirconia films were characterized using complementary techniques of Rutherford backscattering spectroscopy (RBS), glancing-incidence x-ray diffraction (GIXRD), cross-sectional transmission electron microscopy (TEM), selected-area electron diffraction (SAED), secondary-ion mass spectrometry (SIMS), and x-ray photoelectron spectroscopy (XPS). Based on a film thickness of 305 nm observed from TEM and the measured areal density of 2.4×10^{18} atom cm^{-2} determined from RBS, the density of the as-deposited ZrO_2 film is calculated to be ~5.4 g cm^{-3}, which is lower than the theoretical density of 6.045 g cm^{-3} for cubic ZrO_2, partially due to inclusions of argon bubbles in the film resulting from IBAD. The corresponding ion-beam damage profile in displacements per atom (dpa) is calculated with the SRIM 2008.01 full-cascade simulation code[12] using a density of 5.4 g cm^{-3} and threshold displacement energies of 50 eV for both Zr and O atoms, respectively. The average conversion factor over the film thickness from ion fluence 10^{14} cm^{-2} to dose in dpa is ~0.343.

III. RESULTS AND DISCUSSION

A. As-deposited nanostructurally stabilized pure cubic zirconia

Ion-beam-assisted film deposition has a significant contribution to the production of nanostructurally stabilized zirconia in pure cubic phase. It is found that the IBAD technique with a flux of low-energy reactive-gas ions, such as oxygen, to bombard the growing film during deposition, provides one of the most effective techniques to synthesize compound films with improved stoichiometry. Additional bombardment of low-energy nonreactive gas ions, such as argon, during the film growth leads to a substantial relaxation of the residual stress by increasing the mobility of adatoms. Recently, pure cubic phase ZrO_2 in fully nanocrystalline form has also been stabilized by IBAD technique with a size of a few nanometers at room temperature.[4]

The RBS results for the as-deposited zirconia (unirradiated) films are shown in Fig. 1. The results indicate that the films contain primarily Zr and O with an O/Zr ratio close to 2.0. A small amount of Ar exists throughout the zirconia films; no other impurity solutes are detected above the RBS detection limit, which is supported by the SIMS and XPS measurements.

A cross-sectional bright-field TEM image of an as-deposited film is shown in Fig. 2(a), indicating a zirconia film deposited on a Si wafer with a native SiO_2 layer. There are small Ar bubbles with diameter of 1–3 nm observed throughout the films (images are not shown). A high-resolution TEM image of the nanocrystalline zirconia film is shown in Fig. 1(b), where randomly oriented zirconia nanocrystals are evident. The SAED ring pattern in Fig. 1(c) results from a typical polycrystalline structure indicating a fine-grained nanocrystalline film, which is consistent with the TEM image in Fig. 1(d) from a thin section of the as-deposited sample. The cubic structure[3,4] of the film is indicated by the overlaid indices in Fig. 1(c).

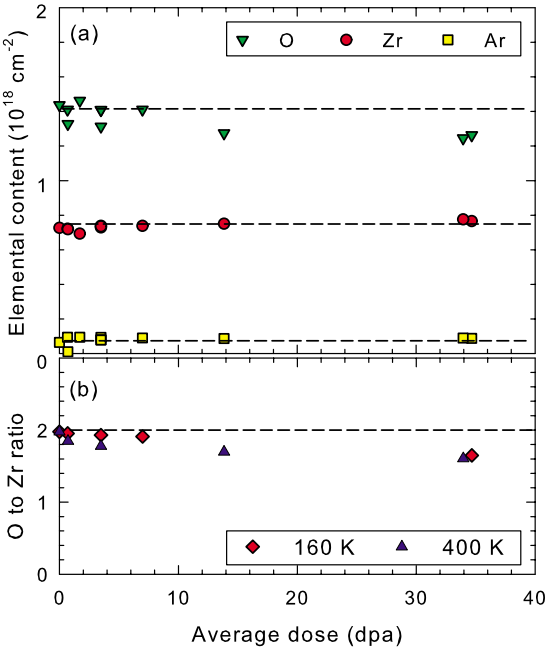

FIG. 1. (Color online) (a) Elemental content change as a function of irradiation dose for all the samples irradiated by 2 MeV Au at 160 and 400 K. (b) The O/Zr ratio as a function of irradiation dose. With increasing ion dose to 35 dpa, the ratio of O to Zr decreases from ~2.0 for the as-deposited films to ~1.65. The dashed lines are horizontal line to guide the eyes.

The as-deposited NSZ film is further evaluated by GIXRD, as shown by the top curves in Fig. 3. The peak positions are in agreement with the results in Fig. 2(c), confirming the cubic phase. The absence of the Bragg peak at $\sim43°$, corresponding to the (102) diffraction maxima from

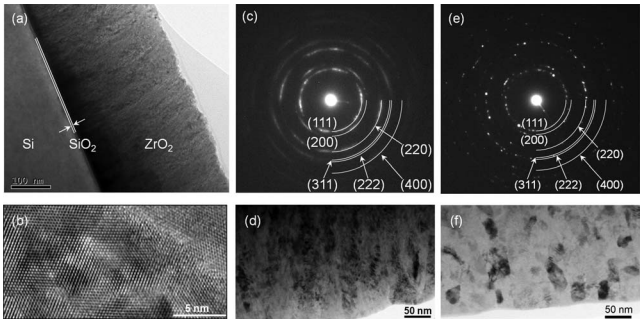

FIG. 2. Characterization of the as-deposited NSZ film: (a) cross-sectional TEM image of the NSZ film on a Si substrate with an interface region of ~4 nm SiO_2, (b) high-resolution TEM image showing randomly oriented nanocrystals and quality of grain boundaries, (c) SAED pattern with overlaid indices of cubic phase and (d) TEM image from a thin section of the film. Characterization of the NSZ film irradiated by 2.0 MeV Au at 160 K to 1×10^{16} cm^{-2}: (e) SAED pattern with overlaid indices of cubic phase and (f) TEM image showing the grain growth.

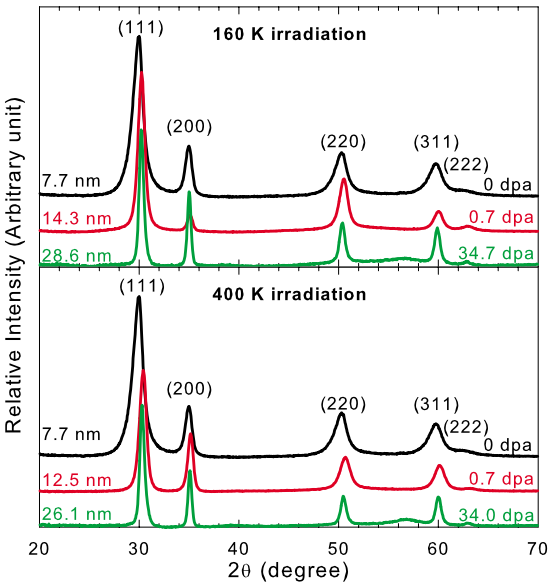

FIG. 3. (Color online) XRD spectra for the as-deposited NSZ film and the films irradiated by 2 MeV Au at 160 K (top plot) and 400 K (bottom plot). The average grain size, irradiation dose, and diffraction indices are marked on the plot.

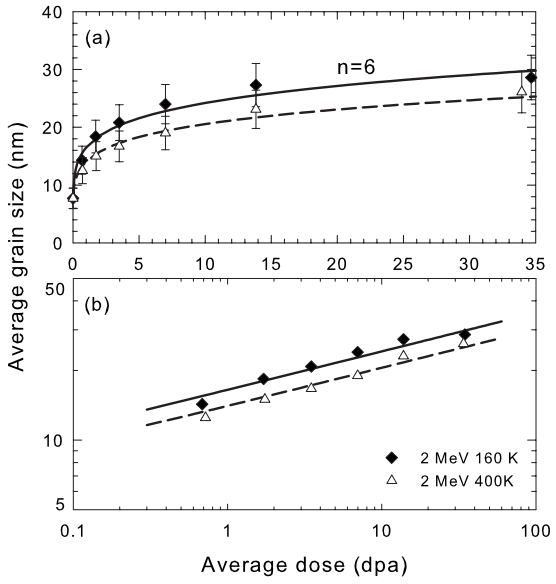

FIG. 4. Grain growth stimulated by 2 MeV Au irradiations at 160 and 400 K. The grain-size variation is within the error bars indicated. The solid and dashed lines are the fits to the expansion of $D^n - D_0^n = K\varphi$ with $n=6$ to guide the eyes. For convenient comparison, the data are shown in both linear (a) and logarithmic (b) scales.

the tetragonal phase, suggests that the tetragonal phase is not present in the ZrO_2 films. Analysis of the (111) peak suggests that the average grain size of the nanocrystalline ZrO_2 film is ~7.7 nm, which is in agreement with the results from high-resolution TEM images, such as the one shown in Fig. 2(b).

B. Phase stability and grain growth under ion irradiation

Phase stability and grain growth are investigated for doses ranging from 0.7 to 35 dpa at 160 and 400 K. A SAED pattern and TEM image for a sample irradiated at 160 K to 1×10^{16} cm^{-2} (34.7 dpa) are shown in Figs. 2(e) and 2(f), respectively. The cubic phase is retained in the irradiated film, as indicated by the overlaid indices in Fig. 2(e). Compared to the SAED pattern in Fig. 2(c), the discrete points in Fig. 2(e) suggest increased grain size and more aligned orientations. Moreover, the growth of nanograins is clearly evident by comparing the image contrast shown in Figs. 2(d) and 2(f).

The XRD spectra of the lowest and highest dose samples at both 160 and 400 K are shown in Fig. 3. For better comparison, low background is removed from all the spectra. All the reflection peaks from the irradiated samples match the cubic reflections of (111), (200), (220), (311), and (222), and these peak positions are in agreement with the indices in Figs. 2(c) and 2(e). No new peak, such as the (102) characteristic peak at ~43° for the tetragonal phase, is observable. Furthermore, the results from Figs. 2(a) and 2(b) show that the widths of all the reflection peaks have become narrower with increasing ion dose, clearly indicating growth of the nanograins.

C. Defect-stimulated grain growth

The irradiation-induced grain growth determined by fitting the (111) peaks from the XRD spectra is summarized in Fig. 4. The experimental uncertainty on averaged grain size determined from the fit to the (111) peak is smaller than 0.2 nm. The large error bars in Fig. 4(a) mainly attribute to the shape of the grains that are elongated along the growth direction. The average grain size increases with irradiation dose; and interestingly, slower grain growth under 400 K irradiation is observed. Recently, an irradiation-induced thermal spike model[13] was proposed to describe grain growth in nanocrystalline metallic foils under ion irradiation. The model, based on the direct impact of the thermal spikes on grain boundaries, is reported to be applicable in a low-temperature regime where grain growth is independent of the irradiation temperature. In this model, grain-boundary migration occurs by atomic jumps, within the thermal spikes, biased by the driving force from local grain-boundary curvature. The model incorporates cascade structure features, such as subcascade formation and the probability of subcascades occurring at grain boundaries. This results in a power law expression, $D^n - D_0^n = K\varphi$, relating the average grain size with the ion fluence, where D_0 is the initial mean grain diameter, φ is ion fluence, n is a constant that may be intrinsic for a material system, and K is proportional to the grain-boundary mobility of the materials and the driving force. The thermal spike model[13] has been applied to grain growth observed in metallic films using *in situ* TEM (where typical sample thickness is a few tens of nanometer and surface effects may not be negligible) over a wide range of irradiation conditions, and an exponent of $n=3$ is found to be in agreement with the experimental observations where $n=1.9-4.3$. This power-law expression is similar to the one that has been used to describe thermal grain growth as a function of annealing time, where $n=2$.[14] Under purely thermal conditions, the atomic jumps across the grain boundary are biased in favor of reducing the grain-boundary curvature, which results in

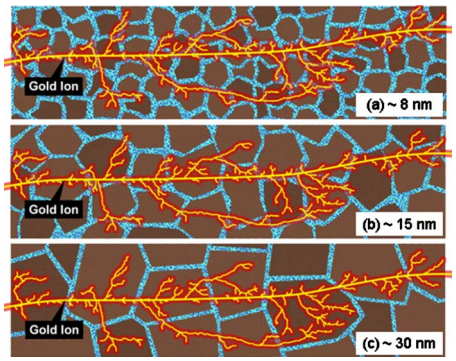

FIG. 5. (Color online) Schematic drawing of the defect-driven mechanism. (a) Average grain size of 8 nm: grain growth is mainly attributed to a large number of defects created from nuclear collision cascades at the grain boundaries, (b) average grain size of 15 nm: grain growth slows down due to significantly less of available defects at the grain boundaries, and (c) ions may pass nanograins with little defects produced at the grain boundaries.

the growth of some larger grains at the expense of smaller ones.

There are similarities between the observations of the grain-growth behavior in the current work and the results from the previous work in metallic systems[13] or under thermal conditions.[14] The lines in Fig. 4 are the power-law fit with $n=6$ to guide the eyes. The slower grain growth at 400 K than that at 160 K, shown in Fig. 4, clearly indicates that irradiation-induced grain growth in ZrO_2 is temperature dependent but not thermally driven.

Under ion irradiation, energy is lost to both atoms and electrons in materials. Kinetic energy transfer to target atoms can result in displacements of atoms from their original sites, thereby forming atomic-scale defects that can migrate and interact with grain boundaries. Energy transfer to target electrons produces electron-hole pairs, and the nonlinear production and transport of electrons and holes can lead to localized electronic excitations and charge at pre-existing defects and interfaces, enhanced defect and atomic diffusion, increased system energy, etc., all of which affect the dynamics of atomic processes and phase transformation dynamics.[15] Since both nuclear and electronic energy loss may contribute to the grain growth, electron irradiations were performed at energies where only ionization occurs without producing displacement damage. Ionization effects on the NSZ films were studied under electron irradiation with energies from 5 to 200 keV. No grain growth were observed, suggesting the essential contribution of irradiation-induced atomic displacement defects to the grain-growth process. A defect-driven mechanism is, therefore, proposed to explain grain-growth behavior in Fig. 4, and a schematic drawing of the processes is shown in Fig. 5. In the defect-driven mechanism, a high concentration of irradiation-induced defects through atomic collision cascades creates a mechanical instability near grain boundaries under nonequilibrium processes. In such an environment, the enhanced defect diffusion results in promoted grain-boundary migration in reducing interface curvature by atomic jumps of the irradiation-induced defects across the grain boundaries, which further lead to grain growth and defect removal.

Ion irradiation leads to a large number of displaced atoms (interstitials) and vacancies that are primarily eliminated by close-pair recombination processes in very short times. The close-pair recombination results in a dynamic equilibrium state with a steady-state concentration of point defects at a given temperature. It is known that defects are more mobile at a higher temperature, which leads to a faster recombination of the interstitials and vacancies, and a lower steady-state concentration of point defects. It has been reported that, in ceramic oxides, the saturation value for the point defect concentration decreases with increasing irradiation temperature, such as in yttria-stabilized cubic single crystalline ZrO_2,[16] $SrTiO_3$,[17] and $Sm_2Ti_2O_7$.[18] Grain growth needs a large steady-state flux of mobile point defects at the grain boundaries. One would expect a lower close-pair recombination rate at 160 K compared to 400 K, and therefore a high steady-state defect concentration to drive grain-growth processes. At 400 K, increased in-grain defect recovery will suppress the grain-growth process, owing to lower defect concentrations.

The different growth behavior, as shown in Fig. 4, indicates the defect dynamics: a closely competing process between the close-pair recombination of irradiation-induced defects and available defects to interact with grain boundaries (both irradiation-induced defects before instantaneous recovery and steady-state point defects). Low instantaneous recombination rate of the displaced atoms and vacancies (the main contributing factor) and high concentration of steady-state point defects (a possible contributing factor) at 160 K may provide the sufficient defects needed for grain-boundary migration and fast grain growth, supporting the defect-driven mechanism proposed in the current work. On the other hand, even though the concentration of steady-state point defects at 400 K is low, the number of the steady-state defects migrating to grain boundaries due to higher temperature may not be less than that at 160 K. Considering instantaneous recombination of large number of irradiation-induced defects and atomic jumps at the grain boundaries are much faster than the migration of the steady-state point defects to the grain boundaries, one may conclude that collision cascades at the grain boundaries play a dominant role in grain growth, and migration of the steady-state defects may be less significant, as described in Fig. 5. At the beginning of the irradiation when the grain size is about 8 nm, as shown in Fig. 5(a), the probability of collision cascades occurring at grain boundaries is high and faster grain growth is attributed mainly to direct collision cascades with typical size less than 10 nm. As the grain size increases to ~15 nm, as shown in Fig. 5(b), the possibility of atomic jumps resulting from direct collision cascades are significantly reduced, and defect migration from a nearby region to grain boundaries may play an important role. As grain size increases to ~30 nm, as shown in Fig. 5(c), reduction in the curvature of grain boundaries and the number of point defects reaching the grain boundaries leads to a slow grain growth. Furthermore, the observed fast grain growth at low dpa may result from an additional process: irradiation-induced sharpening of the amorphous grain boundaries. Such process and irradiation-induced grain growth are occurring somewhat in parallel over some incremental dose range and are not resolvable as separate pro-

cesses. The slow growth at high dpa may also result from enhanced Zener pinning effect due to the existence of small Ar bubbles in the film. The Ar bubbles may act to prevent the motion of grain boundaries by exerting a pinning pressure which counteracts the driving force pushing the boundaries. Under the irradiation, the Ar bubbles appear to be stable in both density and size. As the grain size increases and the density of interfaces decreases, the density of bubble pinning sites on grain boundaries increase and Zener pinning may become important as it may have a strong influence on grain growth, and even lead to a saturation behavior.

D. Oxygen diffusion

Elemental concentrations of Zr, O, and Ar were measured by RBS technique for all the samples that were irradiated by 2 MeV Au ions at 160 and 400 K, and the results as a function of irradiation dose are shown in Fig. 1. While the total amount of Zr and Ar atoms in the films keeps constant, the loss of oxygen with increasing dose is clearly evident. The significant loss of O with increasing dose leads to a decrease in the O/Zr ratio from ~2.0 for the as-deposited films to ~1.65 at a dose of ~35 dpa. The reduction in oxygen in the film is uniformly distributed; no gradients of O/Zr ratio can be determined by RBS, SIMS, or XPS.

Two diffusion mechanisms may be attributed to the significant loss of oxygen, vacancy diffusion, and interstitial diffusion. ZrO_2 is a well-known fast oxygen ionic conductor. The diffusion of the oxygen in zirconia has been attributed to an oxygen-vacancy mechanism, where increased oxygen-vacancy content increases the oxygen ion conductivity. Experimental results indicate that the activation energy for oxygen vacancy migration increases from about 0.5 eV for 8 mol % yttria to 1.3 eV in 30 mol % yttria-stabilized zirconia (YSZ), which is consistent with the results from molecular-dynamics simulations where the oxygen vacancy migration energy ranges from 0.6 to 1.0 eV for 6 to 25 mol % YSZ and about 0.5 eV for 0% yttria.[19] The lowest activation energies (lowest yttria content) are the most relevant to the work presented here. In addition, the diffusion of oxygen in ZrO_2 has also been shown three or four orders of magnitude larger at grain boundaries[20,21] than that in the crystalline bulk. On the other hand, interstitial diffusion is generally faster than vacancy diffusion because bonding of interstitials to the surrounding atoms is normally weaker and there are many more interstitial sites than vacancy sites to jump to. No data on oxygen interstitial migration in cubic ZrO_2 are available. In isostructural cubic UO_2, the activation energy for oxygen-vacancy migration (0.3 eV) is similar to that reported here for ZrO_2; however, the activation energy for a single oxygen interstitial (0.9 eV) is much larger, while the activation energy for a two interstitial cluster is much lower (0.14 eV).[22] While there is a need for theoretical calculations on defect migration energies in nanocrystalline cubic ZrO_2 that is beyond the scope of the present paper, the migration energies for oxygen vacancies and possibly two-interstitial clusters are sufficiently low to contribute to oxygen loss at these irradiation temperatures over the experimental time frames of several hours. Although thermal migration of irradiation-induced defects can contribute to oxygen loss, it is also well known that under highly ionizing irradiation conditions, such as in the present experiments, defect migration can be substantially enhanced by ionization effects associated with the production of a large number of electron-hole pairs, often leading to defect migration and phase transformation kinetics that are dependent on ionization rate and independent of temperature, with activation energies on the order of 0.1 eV.[15,17] Since the oxygen loss appears to be somewhat reversely dependent on temperature, radiation-enhanced interstitial, or vacancy migration, which can be many orders of magnitude over thermal diffusion, may be the dominant processes for oxygen loss in the present experiments.

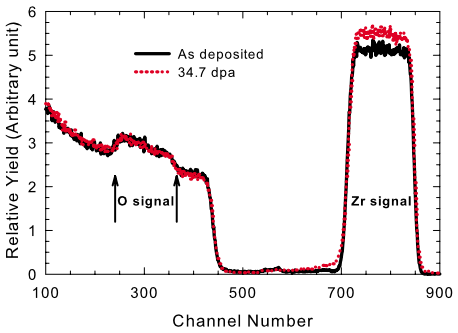

FIG. 6. (Color online) Comparison of RBS spectrum for the as-deposited NSZ film and the film irradiated to 34.7 dpa at 160 K. The same charge is collected.

As the oxygen diffuses through the ZrO_2 film, there are two sites that may act as sinks for oxygen: the free surface and the film/substrate interface. The oxygen atoms that reach the free surface will no longer be tightly bound and are lost while those that diffuse to the interface are trapped in the cavities forming along the interface during the irradiation or becoming available to react with Si to form SiO_2 (results are discussed elsewhere). The loss of oxygen in the NSZ film is also shown in Fig. 6 from the comparison of RBS spectrum between the as-deposited NSZ film and the sample irradiated to 34.7 dpa at 160 K. Due to low sensitivity for the light ion detection, the difference in O content is not obvious. However, higher yield of Zr is evident for the irradiated sample, which indicates a reduced O/Zr ratio. The spatial profile of the oxygen concentration is relatively flat both before and after irradiation. Furthermore, the width and the shape of the O and Zr signals indicate sputtering under the current irradiation condition is negligible, and preferential sputtering of oxygen is unlikely. The enhanced oxygen diffusion in the film and loss of O from the surface may be attributed to the irradiation environment, where enhanced nonequilibrium processes are possible, and unique properties of high-density grain boundaries, such as enhanced chemical decomposition at grain interfaces and irradiation-enhanced surface dissociation. Further study of oxygen behavior as a function of grain size under different irradiation conditions is needed to understand the role of grain boundaries and irradiation-enhanced surface dissociation.

E. Critical size for cubic ZrO_2

The formation of cubic ZrO_2 without chemical stabilizers has been reported for free nanoparticles with diameters of

~2 nm (Ref. 23) or 15 nm (Refs. 24 and 25) and for nanocrystalline films with grain size of 5–8 nm (Ref. 6) or 10 nm.[26] The cubic NSZ films in the current study are crystallographically stable under high-dose irradiation, even when the average size approaches to 30 nm, which is larger than the reported critical size,[6,23–26] above which transformation to the tetragonal or monoclinic polymorph will occur.

Previous results[6,27] have shown that the formation of oxygen vacancies due to local disorder and distortion of the oxygen sublattice is essential for stabilizing nanocrystalline cubic zirconia under annealing. Results from first principle calculations[23] suggest that the difference in total energy between the cubic and tetragonal phases is both size and O/Zr ratio dependent. Nanocrystals of 1.5 nm $Zr_{19}O_{32}$ with O/Zr =1.68 have much lower system energy than those of 2.5 nm $Zr_{225}O_{408}$ with O/Zr=1.81. This implies that, for nanograins of the same size, a higher oxygen-vacancy concentration leads to lower system energy, therefore, a more stable system.

It is important to note that ion irradiation can drive materials far from thermodynamic equilibrium and enable new response pathways of phase transformation and novel scenarios in the dynamic processing of materials. Under irradiation, the stability may derive from interface kinetics, stresses, etc., that give new possibilities for controlling the growth and phase stability of nanostructures. The dependence of average grain size on the O/Zr ratio is shown in Fig. 7, where higher oxygen deficiency is observed in large grains or in the same size grain under higher-temperature irradiation due to higher oxygen diffusivity. High oxygen deficiency (high concentration of oxygen vacancies) may be essential for stabilizing large cubic NSZ grains under high-dose irradiation. The formation of large cubic grains may dependent on energy pathway, rather than representing an energy minimum. Introducing oxygen vacancy by ion irradiation may have significant impact on fuel cell, membrane, and nuclear applications.

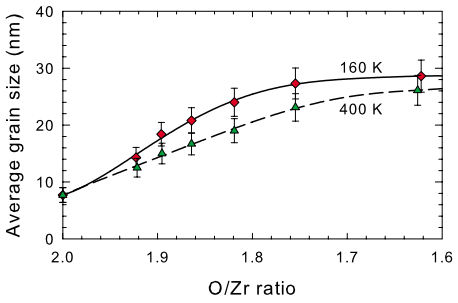

FIG. 7. (Color online) Average grain size as a function of the corresponding O/Zr ratio.

IV. CONCLUSIONS

Grain growth of nanostructurally stabilized cubic zirconia is observed under ion irradiation, which may be attributed to mechanical instability created by a high concentration of irradiation-induced defects near grain boundaries. Slower grain growth observed at 400 K than that at 160 K indicates that the grain growth is not thermally activated and defect-stimulated grain growth is the dominating mechanism. The stability of the cubic phase in large grains may be attributed to an irradiation-induced stable state far from thermodynamic equilibrium. Increase in oxygen vacancies in large grains suggests a possible role of oxygen vacancies in stabilizing nanostructural cubic zirconia.

ACKNOWLEDGMENTS

This research was supported by the Materials Science and Engineering Division, Office of Basic Energy Sciences, U.S. Department of Energy with Battelle and with UT-Battelle, LLC. Experimental work was performed using EMSL, a national scientific user facility sponsored by the Department of Energy's Office of Biological and Environmental Research and located at Pacific Northwest National Laboratory. M. H. Engelhard's effort in XPS measurements is appreciated. Y.Z. is grateful for the discussion with S. J. Zinkle.

*Author to whom correspondence should be addressed, at Oak Ridge National Laboratory, 4500S (A148), MS 6138, Oak Ridge, Tennessee 37831-6138; zhangy1@ornl.gov

[1] A. P. Alivisatos, Science **271**, 933 (1996).
[2] M. V. Kovalenko, M. Scheele, and D. V. Talapin, Science **324**, 1417 (2009).
[3] J. Lian, J. Zhang, F. Namavar, Y. Zhang, F. Lu, H. Haider, K. Garvin, W. J. Weber, and R. C. Ewing, Nanotechnology **20**, 245303 (2009).
[4] F. Namavar, C. L. Cheung, R. F. Sabirianov, W.-N. Mei, X. C. Zeng, G. Wang, H. Haider, and K. L. Garvin, Nano Lett. **8**, 988 (2008).
[5] D. J. Norris, A. L. Efros, and S. C. Erwin, Science **319**, 1776 (2008).
[6] Y. L. Soo, P. J. Chen, S. H. Huang, T. J. Shiu, T. Y. Tsai, Y. H. Chow, Y. C. Lin, S. C. Weng, S. L. Chang, G. Wang, C. L. Cheung, R. F. Sabirianov, W. N. Mei, F. Namavar, H. Haider, K. L. Garvin, J. F. Lee, H. Y. Lee, and P. P. Chu, J. Appl. Phys. **104**, 113535 (2008).
[7] K. E. Sickafus, Hj. Matzke, Th. Hartmann, K. Yasuda, J. A. Valdez, P. Chodak III, M. Nastasi, and R. A. Verrall, J. Nucl. Mater. **274**, 66 (1999).
[8] A. Meldrum, L. A. Boatner, and R. C. Ewing, Phys. Rev. Lett. **88**, 025503 (2001).
[9] A. Benyagoub, Phys. Rev. B **72**, 094114 (2005).
[10] J.-M. Costantini, A. Kahn-Harari, F. Beuneu, and F. Couvreur, J. Appl. Phys. **99**, 123501 (2006).
[11] D. Simeone, G. Baldinozzi, D. Gosset, M. Dutheil, A. Bulou, and T. Hansen, Phys. Rev. B **67**, 064111 (2003).
[12] J. F. Ziegler, SRIM-2008, v. 2008.40, http://www.srim.org
[13] D. Kaoumi, A. T. Motta, and R. C. Birtcher, J. Appl. Phys. **104**, 073525 (2008).

[14] M. Hillert, Acta Metall. **13**, 227 (1965).
[15] Y. Zhang, I.-T. Bae, and W. J. Weber, Nucl. Instrum. Methods Phys. Res. B **266**, 2828 (2008).
[16] K. E. Sickafus, H. Matzke, K. Yasuda, P. Chodak, III, R. A. Verrall, P. G. Lucuta, H. R. Andrews, A. Turos, R. Fromknecht, and N. P. Baker, Nucl. Instrum. Methods Phys. Res. B **141**, 358 (1998).
[17] Y. Zhang, J. Lian, C. M. Wang, W. Jiang, R. C. Ewing, and W. J. Weber, Phys. Rev. B **72**, 094112 (2005).
[18] Y. Zhang, W. J. Weber, V. Shutthanandan, R. Devanathan, S. Thevuthasan, G. Balakrishnan, and D. M. Paul, J. Appl. Phys. **95**, 2866 (2004).
[19] R. Devanathan, W. J. Weber, S. C. Singhal, and J. D. Gale, Solid State Ionics **177**, 1251 (2006).
[20] U. Brossmann, R. Wurschum, U. Sodervall, and H.-E. Schaefer, J. Appl. Phys. **85**, 7646 (1999).
[21] G. Knöner, K. Reimann, R. Röwer, U. Södervall, and H.-E. Schaefer, Proc. Natl. Acad. Sci. U.S.A. **100**, 3870 (2003).
[22] T. Ichinomiya, B. P. Uberuaga, K. E. Sickafus, Y. Nishiura, M. Itakura, Y. Chen, Y. Kaneta, and M. Kinoshita, J. Nucl. Mater. **384**, 315 (2009).
[23] S. Tsunekawa, S. Ito, Y. Kawazoe, and J. T. Wang, Nano Lett. **3**, 871 (2003).
[24] P. Bouvier, E. Djurado, G. Lucazeau, and T. Le Bihan, Phys. Rev. B **62**, 8731 (2000).
[25] M. Gateshki, V. Petkov, G. Williams, S. K. Pradhan, and Y. Ren, Phys. Rev. B **71**, 224107 (2005).
[26] S. C. Moulzolf and R. J. Lad, J. Mater. Res. **15**, 369 (2000).
[27] D. Muñoz Ramo, P. V. Sushko, J. L. Gavartin, and A. L. Shluger, Phys. Rev. B **78**, 235432 (2008).